Human Molecular Genetics, 2017, Vol. 0, No. 0 1–12

doi: 10.1093/hmg/ddx320
Advance Access Publication Date: 14 August 2017
Original Article

ORIGINAL ARTICLE

LRRK2 G2019S-induced mitochondrial DNA damage is LRRK2 kinase dependent and inhibition restores mtDNA integrity in Parkinson's disease

Evan H. Howlett[1], Nicholas Jensen[1], Frances Belmonte[2], Faria Zafar[3], Xiaoping Hu[1], Jillian Kluss[1], Birgitt Schüle[3], Brett A. Kaufman[2], J. T. Greenamyre[1] and Laurie H. Sanders[4,*]

[1]Department of Neurology, Pittsburgh Institute for Neurodegenerative Diseases, [2]Department of Medicine, Center for Metabolism and Mitochondrial Medicine, University of Pittsburgh, Pittsburgh, PA 15260, USA, [3]Parkinson's Institute and Clinical Center, Sunnyvale, CA 94085, USA and [4]Department of Neurology, Duke University Medical Center, Durham, NC 27710, USA

*To whom correspondence should be addressed at: Duke University, 311 Research Drive, 201C Bryan Research Building, Durham, NC 27710, USA. Tel: 9196133890; Fax: 9196846514; Email: laurie.sanders@duke.edu

Abstract

Mutations in *leucine-rich repeat kinase 2* (*LRRK2*) are associated with increased risk for developing Parkinson's disease (PD). Previously, we found that LRRK2 G2019S mutation carriers have increased mitochondrial DNA (mtDNA) damage and after zinc finger nuclease-mediated gene mutation correction, mtDNA damage was no longer detectable. While the mtDNA damage phenotype can be unambiguously attributed to the LRRK2 G2019S mutation, the underlying mechanism(s) is unknown. Here, we examine the role of LRRK2 kinase function in LRRK2 G2019S-mediated mtDNA damage, using both genetic and pharmacological approaches in cultured neurons and PD patient-derived cells. Expression of LRRK2 G2019S induced mtDNA damage in primary rat midbrain neurons, but not in cortical neuronal cultures. In contrast, the expression of LRRK2 wild type or LRRK2 D1994A mutant (kinase dead) had no effect on mtDNA damage in either midbrain or cortical neuronal cultures. In addition, human LRRK2 G2019S patient-derived lymphoblastoid cell lines (LCL) demonstrated increased mtDNA damage relative to age-matched controls. Importantly, treatment of LRRK2 G2019S expressing midbrain neurons or patient-derived LRRK2 G2019S LCLs with the LRRK2 kinase inhibitor GNE-7915, either prevented or restored mtDNA damage to control levels. These findings support the hypothesis that LRRK2 G2019S-induced mtDNA damage is LRRK2 kinase activity dependent, uncovering a novel pathological role for this kinase. Blocking or reversing mtDNA damage via LRRK2 kinase inhibition or other therapeutic approaches may be useful to slow PD-associated pathology.

Introduction

Parkinson's disease (PD) is the most common neurodegenerative movement disorder and over ten million people worldwide are living with PD. Most PD cases are sporadic and only 10% of PD patients report a family history. Of those, mutations or risk factors can be identified in up to 50% (1). The most common cause of inherited PD is autosomal dominant mutations in *leucine-rich repeat kinase 2* (*LRRK2*). Most pathogenic mutations are located in the *LRRK2* kinase or GTPase domain. Though both the normal and pathological functions of LRRK2 are unknown,

Received: May 30, 2017. **Revised:** July 21, 2017. **Accepted:** August 10, 2017

current evidence supports a role for LRRK2 kinase activity in the pathogenesis of PD (2,3). The NM_198578.3 (*LRRK2*): c.6055 G > A (p.Gly2019Ser) mutation in the kinase domain leads to an increase in catalytic activity by about three fold and is thought to underlie its neurotoxic effect (4–6). Consequently, great efforts have focused on the development of potent and selective inhibitors of LRRK2 kinase activity (7–11). Treatment with LRRK2 kinase inhibitors both *in vitro* and *in vivo* (12–14) have demonstrated an ability to mitigate toxicity and neurodegeneration, with unclear off-target effects (15,16). However, the mechanism(s) of action or specific targets by which LRRK2 inhibitors provide therapeutic benefit are unknown.

There is accumulating evidence for neurological syndromes that are caused by a DNA repair deficiency (17). Just recently, a newly identified human neurodegenerative disease, that presented with ocular motor apraxia, axonal neuropathy and progressive cerebellar ataxia, was due to a mutation in single-strand break repair (18). This highlights that functional DNA repair pathways are crucial for the maintenance of neural homeostasis. How DNA damage and repair defects lead to degeneration is a complex question and one that requires much effort in future studies (19). However, the significance of unrepaired neuronal mitochondrial DNA (mtDNA) damage in the pathogenesis of age-related diseases is largely unexplored, but is emerging as playing a role in PD (20–22).

Previously, we found that LRRK2 G2019S mutation carriers have increased mtDNA damage in human induced pluripotent stem cell (iPSC)-derived differentiated neuroprogenitor and neural cells (21). Importantly, when the mutation is corrected with zinc finger nuclease-mediated gene editing, mtDNA damage is no longer detectable. Thus, the mtDNA damage phenotype can be unambiguously attributed to the LRRK2 G2019S mutation (21), though its precise mechanism remains elusive. In the present study, we examine the role of LRRK2 kinase function in LRRK2 G2019S-mediated mtDNA damage, using both genetic and pharmacological approaches in cultured neurons and PD patient-derived cells. Our results suggest that aberrant LRRK2 kinase activity is a critical underlying mechanism in the accumulation of LRRK2 G2019S induced-mtDNA damage.

Results

New LRRK2 G2019S *in vitro* primary neuronal model

Though many LRRK2 cell line models exist, the regulation of PD phenotypes, particularly mitochondrial, may be neuron-specific (23). In order to better understand the normal and pathological functions of LRRK2 that may underlie the mechanisms of LRRK2 G2019S-mediated mtDNA damage, we developed a new *in vitro* model. Primary midbrain neuronal cultures from E17 Sprague Dawley rats were virally transduced with green fluorescence protein (GFP) fused to the C-terminus of full-length human wild-type LRRK2, LRRK2 G2019S (increased kinase activity mutant), or LRRK2 D1994A (kinase dead) mutant using the BacMam gene delivery system based on a modified insect cell baculovirus. The BacMam system was chosen due to the reproducible and consistent transduction and transgene expression of the large LRRK2 target (24).

To validate our LRRK2 primary neuronal model, we confirmed the expression of full-length LRRK2 by performing western blotting using an anti-pan LRRK2 antibody. Primary midbrain neuronal cultures expressing either LRRK2 wild type, LRRK2 G2019S or LRRK2 D1994A mutant each had a similar five-fold increase in LRRK2 expression relative to GFP-expressing cultures (Fig. 1A and B). Since the anti-pan LRRK2 antibody recognizes both the human and rat LRRK2 protein, we performed quantitative RT-PCR to assess the effect of BacMam viral transduction on human and rat *LRRK2* transcripts. Similar to the western blot results, qRT-PCR revealed similar transcript levels of human *LRRK2* in primary midbrain neuronal cultures expressing either LRRK2 G2019S or LRRK2 D1994A when compared to LRRK2 wild type (Fig. 1C). Endogenous levels of rat *LRRK2* transcripts were unaffected by the transduction with human BacMam vectors (Fig. 1D). Overall, the BacMam gene delivery system efficiently expressed similar levels of wild type and mutant variants of LRRK2, which allows direct comparisons of phenotypes.

Degeneration of neuronal processes occurs early in PD pathogenesis (25,26). Retracted or shortened neurites with overexpression of LRRK2 G201S9S in neurons have been reported by several groups (27,28). To determine if LRRK2-expressing neurons display neurite shortening in our model, LRRK2 wild type, LRRK2 G2019S or LRRK2 D1994A mutant were transduced into primary midbrain neurons for 24 h. Decreased neurite length was found in primary midbrain neuronal cultures expressing LRRK2 G2019S relative to GFP, LRRK2 wild type or the LRRK2 D1994A mutant (Fig. 1E). Overexpression of LRRK2 wild type or LRRK2 D1994A did not induce neurite shortening (Fig. 1E), consistent with previous work (29). Transduction with LRRK2 wild type, LRRK2 G2019S or the LRRK2 D1994A mutant did not affect cell viability compared to GFP-expressing primary midbrain neurons (Fig. 1F). Lastly, no difference in cellular viability was observed when GFP-expressing primary midbrain neuronal cultures were compared to non-transduced cultures (Supplementary Material, Fig. S1).

Complex I inhibition and decreased mitochondrial respiration are considered to be an important component to the pathogenesis of PD (30,31). We measured oxygen consumption rates (OCR) in primary neurons transduced with GFP, LRRK2 wild type, LRRK2 G2019S or LRRK2 D1994A mutant in response to oligomycin (inhibitor of ATP synthase), carbonyl cyanide 4-trifluoromethoxy phenylhydrazone, (FCCP, the proton ionophore) and rotenone combined with antimycin A (a mitochondrial complex I inhibitor and III inhibitor respectively). Consistent with previous published results (13), the basal OCR and ATP-linked respiration of primary neurons expressing LRRK2 G2019S was reduced compared to GFP-expressing cultures (Fig. 2A–C). The impact of overexpression of LRRK2 wild type or LRRK2 D1994A kinase inactivating mutant on mitochondrial respiration has not been investigated (14,27). LRRK2 wild type and GFP expressing neuronal cultures showed similar basal respiration and changes in OCR in response to oligomycin, FCCP, and rotenone and antimycin A (Fig. 2A). Remarkably, the LRRK2 D1994A kinase dead mutant showed decreased basal respiration and ATP-linked respiration relative to GFP-expressing cultures (Fig. 2A–C). While the mechanism for this observation is unclear and requires further investigation, the PD LRRK2 *G2385R* risk factor which causes a partial loss of kinase function, still interestingly correlates with PD cellular phenotypes (29,32). Nonetheless, we have developed a new *in vitro* primary neuronal model that recapitulates many of the alterations associated with the LRRK2 G2019S mutation (13,33).

Regionally selective LRRK2 G2019S-induced mtDNA damage

In order to test the effects of wild type or mutant LRRK2 on mtDNA damage levels, DNA was purified from primary

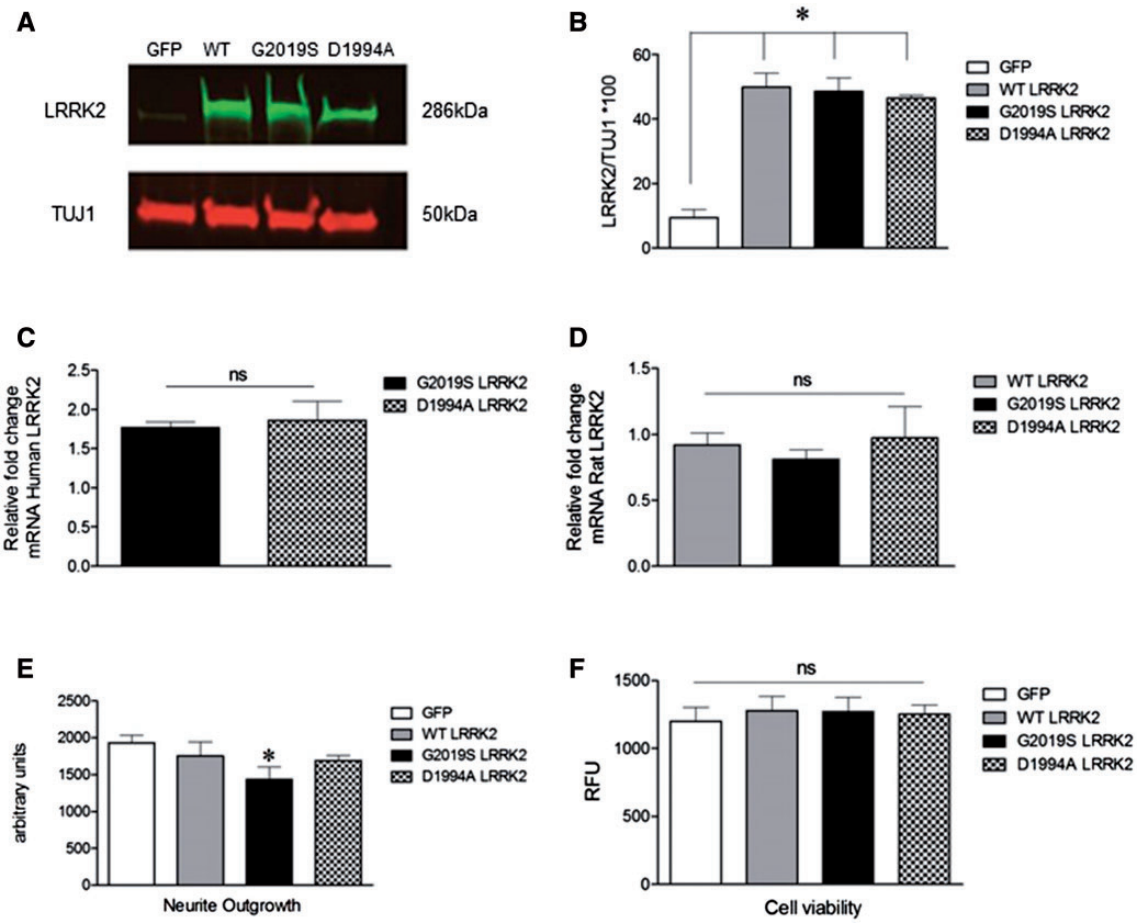

Figure 1. LRRK2 *in vitro* primary midbrain neuronal model. (**A**) Representative western blots of transduced midbrain neuronal cells show expression of full-length LRRK2 blotted with antibodies raised against LRRK2. TUJ1 was blotted as a loading control. (**B**) Quantification of western blots demonstrate a five-fold increase of LRRK2 expression with transduction of LRRK2 wild type, G2019S or D1994A compared to GFP expressing cultures. (*$P < 0.05$, determined by one-way ANOVA with a Tukey's posthoc comparison). (**C**) qRT-PCR revealed similar transcript levels of human or (**D**) rat *LRRK2* in primary midbrain neuronal cultures expressing either LRRK2 wild-type, LRRK2 G2019S or LRRK2 D1994A. (**E**) LRRK2 G2019S expressing cultures displayed a neurite outgrowth defect relative to GFP expressing cultures. (*$P < 0.05$, determined by one-way ANOVA with a Bonferroni's posthoc multiple comparison). (**F**) Cell viability was comparable across all groups. All experiments were performed with three biological replicates and data are presented as mean ± SEM.

midbrain neurons expressing GFP, LRRK2 wild type, LRRK2 G2019S or LRRK2 D1994A. To measure mtDNA damage, we used a quantitative polymerase chain reaction (PCR)-based assay that we have successfully applied to various different cell types (20–22). Briefly, the assay involves amplification of a PCR fragment specific to the mitochondrial genome. Less PCR product will be produced when mtDNA damage or lesions block the ability of the DNA polymerase to replicate. Thus, mtDNA damage or mtDNA repair intermediates that slow down or impair DNA polymerase progression will be detected. If equal amounts of DNA are amplified under identical conditions, then PCR products can be compared from experimental and control conditions.

We found that mtDNA damage was significantly increased in primary midbrain neurons expressing LRRK2 G2019S relative to GFP-expressing cultures (Fig. 3A). In contrast to the LRRK2 G2019S mutant, mtDNA damage was not detected in LRRK2 wild type or LRRK2 D1994A mutant expressing neuronal cultures compared to GFP-expressing cultures (Fig. 3A).

Since wild type or mutant LRRK2 might alter levels of mtDNA, we assayed for mtDNA copy number. Mitochondrial DNA copy number was similar across all viral transduction conditions (Fig. 3B). Thus, the extent of mtDNA damage in wild type or mutant LRRK2 expressing midbrain neurons was not related to changes in mtDNA steady state levels. These data suggest that accumulating mtDNA damage depends on LRRK2 kinase activity and not LRRK2 levels.

We reported that in both rotenone PD rat models and human postmortem brain tissue that mtDNA damage specifically persists in midbrain neurons, but not in cortex (22). To determine whether LRRK2 G2019S-induced mtDNA damage is similarly brain region specific, we assessed mtDNA damage in primary cortical neurons expressing either GFP, LRRK2 wild type, LRRK2 G2019S or LRRK2 D1994A. In contrast to midbrain neurons, mtDNA damage was not detected in LRKK2 G2019S compared to GFP, LRRK2 wild type, or LRRK2 D1994A expressing primary cortical neuronal cultures (Fig. 3C). Mitochondrial DNA copy number was comparable in cortical neuronal cultures expressing GFP relative to LRRK2 wild type, LRRK2 G2019S and LRRK2 D1994A (Fig. 3D). Lack of detectable mtDNA damage was not due to changes in cell death, as GFP, LRRK2 wild type, LRRK2 G2019S and LRRK2 D1994A cortical cultures had similar cell viability (Fig. 3E). Interestingly, no differences in neurite length were detected when comparing GFP, LRRK2 wild type, LRRK2 G2019S and LRRK2 D1994A cortical cultures (Fig. 3F). In conclusion, expression of

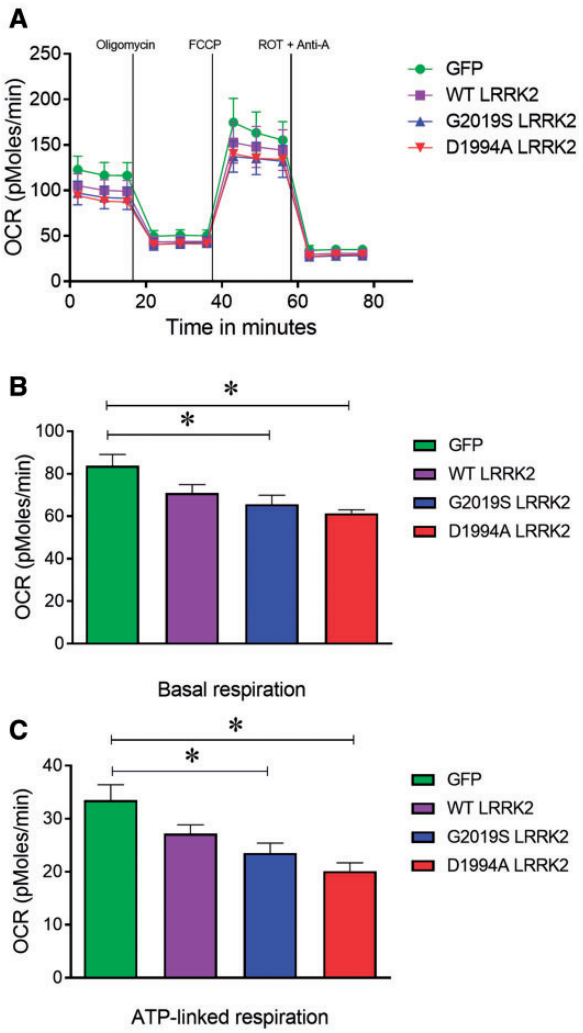

Figure 2. Overexpression of LRRK2 mutants impaired mitochondrial respiration in rat primary midbrain neurons *in vitro*. Oxygen consumption rates (OCR) were compared in GFP-expressing cultures to (**A**) LRRK2 wild-type, LRRK2 G2019S or LRRK2 D1994A expressing midbrain neuronal cultures. (**B**) Expression of LRRK2 G2019S and D1994A decreased basal OCR (**C**) and ATP-linked respiration relative to GFP expressing cultures. Data are presented as mean ± SEM for at least three biological replicates. (*$P < 0.05$, determined by one-way ANOVA with a Tukey's posthoc comparison).

LRRK2 G2019S-induced mtDNA damage selectively in midbrain, but not in cortical neuronal cultures.

Pharmacologically inhibiting LRRK2 kinase activity restores mtDNA damage to control levels in primary midbrain neuronal cultures

To further test whether LRRK2 G2019S-induced mtDNA damage is kinase dependent, we used an acute pharmacological inhibition approach by investigating the effects of the LRRK2 kinase inhibitor GNE-7915 on mtDNA damage (34–36). We first used a pretreatment paradigm in which primary midbrain neuronal cultures were treated with vehicle or GNE-7915 for 24 h and then transduced with either GFP or LRRK2 G2019S for 24 h. After 48 h total of treatment, cell pellets were collected, DNA extracted and the mtDNA damage analysis performed. Pretreatment with GNE-7915 was able to prevent LRRK2 G2019S-induced mtDNA damage (Fig. 4A). Mitochondrial DNA copy number was unaffected by treatments (Fig. 4B). Importantly, treatment of GNE-7915 by itself did not alter mtDNA damage levels or copy number (Supplementary Material, Fig. S2). We also confirmed that treatment with GNE-7915 reduced levels of LRRK2 pSer935, as these sites may be modulated indirectly by LRRK2 kinase activity (37,38) and dephosphorylation occurs with LRRK2 kinase inhibitor exposure (39,40) (Supplementary Material, Fig. S3).

Primary midbrain neurons were then simultaneously transduced with either GFP or LRRK2 G2019S and treated with vehicle or GNE-7915 for 24 h. In this cotreatment paradigm, LRRK2 G2019S-induced mtDNA damage was abrogated (Fig. 4C), while mtDNA copy number remained unaffected by treatments (Fig. 4D).

Since we were able to confirm that both pretreatment and cotreatment with GNE-7915 prevents or abrogates mtDNA damage, we next treated with the LRRK2 kinase inhibitor after transduction with GFP or LRRK2 G2019S to examine whether mtDNA damage could be reversed. Primary neurons were transduced with GFP or LRRK2 G2019S for 18 h and then exposed to vehicle or GNE-7915 for 6 h. After 24 h total of treatment, cell pellets were collected, DNA extracted and the mtDNA damage analysis performed. Most strikingly, in this posttreatment paradigm, exposure to GNE-7915 was able to restore mtDNA damage to control levels (Fig. 4E). Mitochondrial DNA copy number was unaffected by treatments (Fig. 4F). Levels of mtDNA damage were confirmed to be increased in primary midbrain neuronal cultures expressing LRRK2 G2019S for 18 h relative to GFP-only expressing cultures (Supplementary Material, Fig. S4). Overall, these results not only implicate kinase activity as part of the LRRK2 G2019S-induced mtDNA damage underlying mechanism, but that mtDNA damage levels may be sensitive to clinically relevant therapeutic interventions.

PD patient-derived cells harboring the LRRK2 G2019S mutation display increased mtDNA damage and LRRK2 kinase inhibition restores mtDNA integrity to healthy control levels

To extend and validate our observations from our LRRK2 overexpression neuronal toxicity model and determine its wider applicability to human cells with endogenous LRRK2 levels, we used an acute pharmacological LRRK2 inhibition approach using PD patient-derived cells. We examined control and PD patient derived Epstein-Barr virus (EBV)-transformed lymphoblastoid cell lines (LCL); detailed demographic information can be found in (Table 1). Levels of mtDNA damage were compared in LCLs from healthy controls and PD patient LRRK2 G2019S carriers. Mitochondrial DNA damage was increased in LRRK2 G2019S patient-derived LCLs compared to age-matched healthy controls (Fig. 5A). Mitochondrial DNA copy number was not different between LRRK2 G2019S patient-derived LCLs compared to age-matched healthy controls (Fig. 5B). Increased mtDNA damage in LRRK2 G2019S patient-derived LCLs did not correlate with LRRK2 RNA (Supplementary Material, Fig. S5) or protein levels (Supplementary Material, Fig. S6). Furthermore, the accumulation of mtDNA damage was not associated with a concomitant increase in mtDNA deletions (Fig. 5C).

Next, we tested whether culturing LCLs in the presence of a selective LRRK2 kinase inhibitor would affect mtDNA damage levels. Exposure of LRRK2 G2019S patient-derived LCLs to GNE-7915 restored mtDNA damage to control levels with 24 h of exposure (Fig. 6A), without a change in mtDNA copy number (Fig.

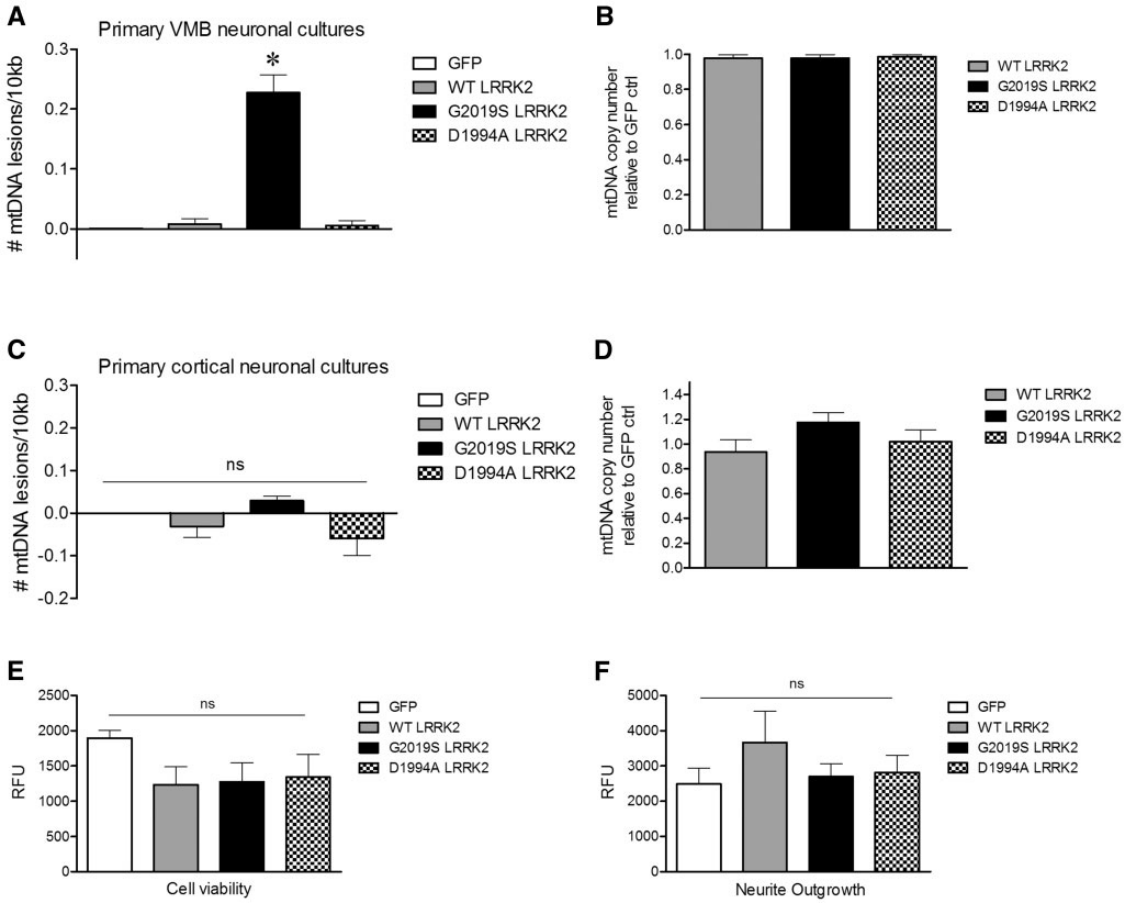

Figure 3. Overexpression of LRRK2 G2019S induced mtDNA damage in rat primary midbrain but not cortical neuronal cultures *in vitro*. (**A**) Primary midbrain neuronal cultures expressing GFP, LRRK2 wild type, LRRK2 G2019S or LRRK2 D1994A were analyzed for mtDNA damage. (*$P < 0.05$, determined by one-way ANOVA with a Tukey's posthoc comparison). (**B**) LRRK2 wild type or mutant overexpression did not change mtDNA copy number in midbrain neuronal cultures. (**C**) In contrast, LRRK2 wild type or mutants had no effect on mtDNA damage levels in rat primary cortical neuronal cultures, or (**D**) alter mtDNA copy number. (**E**) In these cortical cultures, LRRK2 wild type or mutant overexpression did not change viability relative to GFP expressing cultures. (**F**) Neurite outgrowth was unchanged with LRRK2 overexpression compared to GFP expressing cortical cultures. Data are presented as mean ± SEM. The PCR-based assay was performed in technical triplicate (twice) for each biological replicate ($n = 3$). Cell viability and neurite outgrowth experiments were performed with three biological replicates.

6B). GNE-7915 treatment for 24 h resulted in reduction of LRRK2 pSer935 levels (Supplementary Material, Fig. S7).

Lastly, we investigated whether there is peripheral cell-type specificity for LRRK2 G201S-induced mtDNA damage in human derived cells. Fibroblasts obtained from LRRK2 G2019S mutation carriers, when challenged with stressors, demonstrate mitochondrial phenotypes (13,41). Therefore, we carried out experiments to determine if PD patient-derived fibroblasts harboring the LRRK2 G2019S mutation accumulate mtDNA damage. Fibroblasts were obtained from three PD patients carrying the heterozygous LRRK2 G2019S mutation and three age-matched healthy subjects (Table 2). No differences in mtDNA damage levels between healthy subjects and LRRK2 G2019S mutation carriers were detected in fibroblasts (Table 2). This is consistent with our previous findings in a single fibroblast cell line (21). In addition, mtDNA copy number was similar across all fibroblast cell lines (Table 2).

Discussion

The mechanism by which increased LRRK2 kinase activity mediates PD-associated toxicity remains unclear. The objective of our study was to understand whether LRRK2 kinase function is playing a role in LRRK2 G2019S mediated mtDNA damage. Our data demonstrate that mtDNA damage is induced only by the PD-associated G2019S mutation in *LRRK2*, and not with wild type or kinase-dead *LRRK2*. The mtDNA damage phenotype can be functionally prevented or restored by pharmacological treatment with a LRRK2 kinase inhibitor in a LRRK2 neuronal model and PD patient-derived cells. These results revealed that aberrant kinase activity is likely playing a critical role in the underlying mechanism in mtDNA damage accumulation – and perhaps in the pathogenesis of PD. This new link between LRRK2 kinase activity and mtDNA damage have implications for the pathologic actions that underlie LRRK2 G2019S associated PD, as well as LRRK2 kinase based therapeutics.

The function of LRRK2 is likely to be pleiotropic in nature, shown to be involved in neurodegeneration and in more peripheral processes, including kidney and lung function, in rats and mice (15,42). Therefore, the role of the LRRK2 kinase in PD pathogenesis is presently unclear (43). Towards identifying the function of LRRK2, a phosphoproteomics screen was undertaken and revealed Rab10 and other members of the Rab GTPase family to be direct substrates of LRRK2 (44). While we discovered that LRRK2 G2019S induced mtDNA damage is LRRK2 kinase activity dependent, the specific signaling pathway responsible for

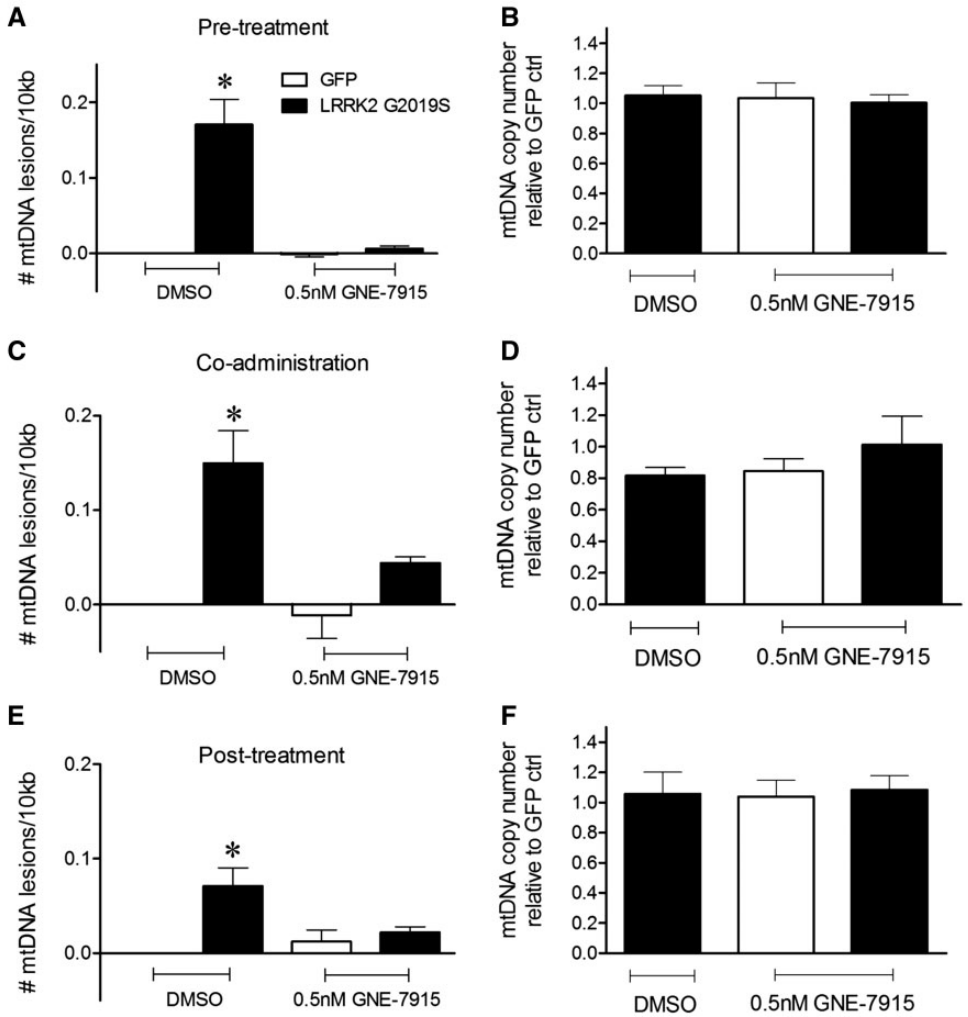

Figure 4. Mitochondrial DNA damage in primary neurons expressing human LRRK2 G2019S exposed to a LRRK2 kinase inhibitor was prevented or reversed to normal levels. Primary midbrain neurons expressing either GFP or human LRRK2 G2019S were either (**A**) pre-treated, (**B**) co-treated or (**C**) post viral transduction treated with a very low dose of LRRK2 kinase inhibitor GNE-7915 (0.5 nM). (*$P < 0.05$, determined by one-way ANOVA with a Tukey's posthoc comparison). Experiments were conducted with at least three biological replicates. The PCR-based assay was performed in technical triplicate (twice) for each biological replicate.

this phenotype is undetermined. Membrane trafficking defects in PD via loss of function mutations in VPS35 lead to mitochondrial fragmentation and dysfunction (45). Perhaps enhanced LRRK2 kinase activity and the resulting increased phosphorylation of Rab GTPases leads to intracellular trafficking defects that ultimately cause mitochondrial dysfunction and mtDNA damage. It will be important to fully explore the role of Rabs and other newly identified LRRK2 substrates in LRRK2 G2019S mediated mtDNA damage.

Given its potential central role in both genetic and idiopathic PD, LRRK2 is an attractive therapeutic target. Protection against LRRK2 or alpha-synuclein-induced pathology or toxicity has been shown by inhibition of LRRK2 kinase activity either pharmacologically or genetically (5,6,14,28). These results and others highlight the preventative or disease-modifying therapeutic potential of LRRK2 kinase inhibitors (7,46). Assuming these LRRK2 kinase inhibitors are deemed safe and efficacious and human trials are initiated, whether to include LRRK2 mutation carriers and/or idiopathic PD subjects in clinical trials is a matter of debate. Surprisingly, we found that LRRK2 kinase inhibition was able to abrogate mtDNA damage, regardless of the timing of exposure (i.e. prior to, concurrently with or post the presence of LRRK2 G2019S-induced mtDNA damage). Our results suggest that LRRK2 inhibitors could be administered to PD patients even after pathology is present and still reap a therapeutic benefit. What's more, it is tantalizing to entertain the idea that if asymptomatic LRRK2 G2019S mutation carriers were treated with LRRK2 kinase inhibitors, mtDNA could even be prevented. Furthermore, there is currently little known about the role of the LRRK2 kinase activity in idiopathic PD (3). In light of our previous observations of increased mtDNA damage in human idiopathic postmortem substantia nigra brain samples (22), future studies may investigate whether mtDNA damage in non-familial PD is LRRK2 kinase dependent.

Mitochondrial DNA has been thought to be more susceptible to DNA damage than its nuclear DNA counterpart (47). Mitochondrial DNA damage and mitochondrial mutations are distinct biochemical alterations, and whether the damage to mtDNA in PD leads to mtDNA mutations is unclear (30,48). We employed droplet digital PCR (dPCR) assays to investigate whether the increased mtDNA damage we observed with *LRRK2* G2019S was also associated with an increase in mtDNA

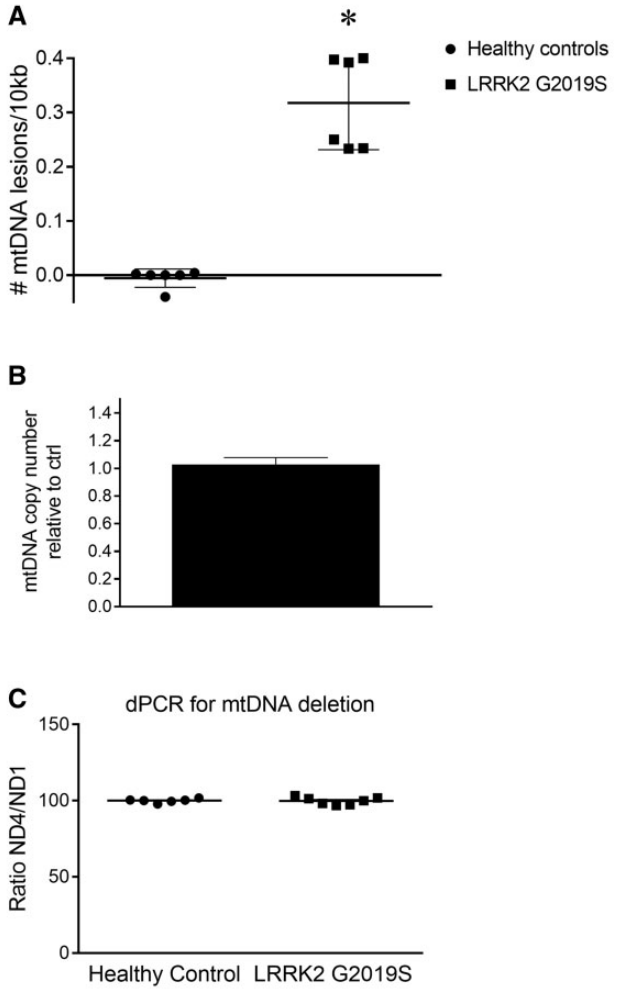

Figure 5. Mitochondrial DNA damage was increased (but not mtDNA deletions) in PD patients that harbor the LRRK2 G2019S mutation. (**A**) Mitochondrial DNA damage was increased in LRRK2 G2019S patient-derived LCLs ($n = 6$) compared to age-matched healthy controls ($n = 6$). (*$P < 0.001$, determined by Student-t test). The PCR-based assay was performed in technical triplicate (twice) for each biological replicate. Data are presented as mean ± SEM. (**B**) The differences in mtDNA damage in control vs LRRK2 G2019S LCLs were not attributable to changes in steady state mtDNA levels. (**C**) dPCR was performed to assay for mtDNA deletions in LRRK2 G2019S mutation carriers and age-matched healthy controls. Each sample group was comprised of six or seven subjects. Each individual sample was measured in technical triplicate and averaged.

deletions. The dPCR approach we used has improved mtDNA deletion sensitivity relative to traditional semi-quantitative methods (49). We did not find that the burden of mtDNA damage due to LRRK2 G2019S was converted to a significant level of mtDNA deletions. However, our interpretation is only limited to mtDNA deletions and future investigations may evaluate mtDNA base substitutions. Our current results that mtDNA damage does not readily convert into mutations is consistent with a recent study that mtDNA is resistant to mutations even in the presence of high levels of mitochondrial adducts (50).

One of the major questions that still remains in the PD field is the basis for the selective neuronal vulnerability in PD. Many studies have focused their attention on Lewy pathology as a driver of neuronal dysfunction and death. However, analysis of human post mortem brains revealed that while some LRRK2 G2019S carriers show Lewy pathology - not all do (51). This suggests, that Lewy pathology is not required for nigral degeneration in LRRK2-related PD. Other factors have been proposed to contribute to selective neuronal loss, including a role for Cav1 channels (52). Here, we show that overexpression of LRRK2 G2019S only induces mtDNA damage in the vulnerable midbrain neuronal population and not in cortical neurons. This is reminiscent of our similar findings in rotenone models and human post-mortem brain tissue in which mtDNA damage accumulates selectively in nigral dopamine neurons in idiopathic PD (22). Perhaps, the most salient question is why does mtDNA damage manifest in some cell types (primary midbrain neurons that overexpress LRRK2 G2019S, LRRK2 G2019S patient-derived LCLs, LRRK2 G2019S iPSC-derived differentiated neuroprogenitor and neural cells), but not others (undifferentiated iPSCs, fibroblasts or cortical neurons) (21)? The underlying mechanism for this vulnerability or resistance to LRRK2 G2019S mutation induced mtDNA damage is completely unknown. Possible contributing factors may be related to redox signaling (53), oxidative stress (30), dopamine metabolism (54), LRRK2 expression levels (15) or rab phosphorylation (44) and is an exciting new avenue for mechanistic exploration. We now have models in which to test pathways responsible for the preferential accumulation of mtDNA damage in different cell populations, which may lend insight into neuronal vulnerability in PD.

Measurement of LRRK2 dephosphorylation at constitutive phosphorylation sites has been the most widely used assay as a potential pharmacodynamic biomarker of LRRK2 kinase inhibition (38,55). However, these residues (LRRK2 Ser910, Ser935, Ser955 and Ser973) are not direct LRRK2 autophosphorylation sites and rather are regulated indirectly by LRRK2 kinase activity (37,38). Under conditions that reverse mtDNA damage, it is unclear and remains to be determined which autophosphorylation and/or other phosphorylation sites within LRRK2 are affected. Determining whether mtDNA damage restoration is a direct or indirect result of LRRK2 kinase activity will be important to further our understanding of the biological role of this kinase. Overall, we have discovered that the mtDNA damage phenotype following treatment with LRRK2 inhibitors may be a good candidate to measure target engagement, and future studies investigating its utility are warranted.

In summary, the findings from our study indicate that the mtDNA damage accumulation as a result of the LRRK2 G2019S mutation is kinase activity dependent. Furthermore, targeting mtDNA damage via LRRK2 kinase inhibition holds significant promise for treating PD.

Materials and Methods

Rat primary midbrain and cortical neuron cultures and transfections

Primary cultures were prepared following previously published protocols (22,56,57) with minor modifications. Ventral midbrain or cortical tissues were dissected from E17 Sprague Dawley rat brains. Pooled ventral midbrain or cortical tissues were dissected in L-15 medium: (Leibovitz's 1X medium (Invitrogen), and penicillin-streptomycin (200 units, Cellgro) and enzymatic digestion performed using trypsin (1X trypsin–ethylenediaminetetraacetic acid (EDTA) at 37 °C for 20 min). Cell number was evaluated using the trypan blue assay and a hemocytometer. Cells were dissociated by mild mechanical trituration with a Pasteur pipette and seeded with a repeating pipette on circular coverslips (Fisher Scientific, 12-545-82) pre-coated with PDL (0.1 mg/ml) in 24-well culture plates at a density of 5×10^5 cells/well (midbrain) or 1×10^5 cells/well

Table 1. Lymphoblastoid cell lines: genotypes, individual age at biopsy, gender, clinical status, and ID numbers

Cell line ID #	Age at biopsy	Genetic mutation	Clinical Status	Gender
ND02559	46	None detected	Unaffected	M
ND01618	46	*LRRK2* G2019S heterozygous	Affected	M
ND02760	60	None detected	Unaffected	F
ND00045	60	*LRRK2* G2019S heterozygous	Affected	F
DT-025	60	*LRRK2* G2019S heterozygous	Affected	F
ND03000	68	*LRRK2* G2019S heterozygous	Affected	F
ND00312	72	None detected	Unaffected	M
ND02752	72	*LRRK2* G2019S heterozygous	Affected	M
ND00011	75	None detected	Unaffected	F
ND00264	75	*LRRK2* G2019S heterozygous	Affected	F
MN-053	76	None detected	Unaffected	F
BGK-055	79	None detected	Unaffected	F

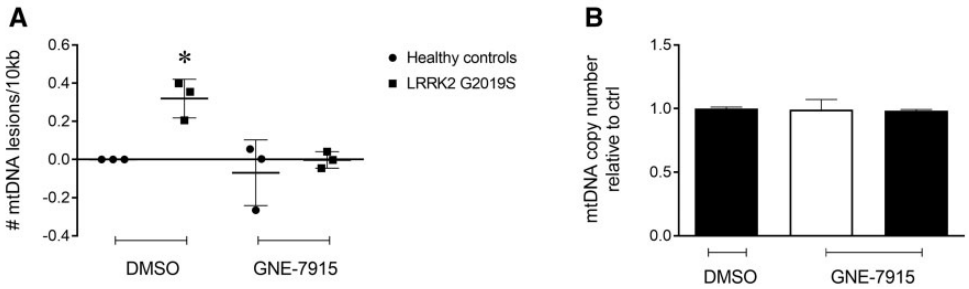

Figure 6. LRRK2 kinase inhibitor exposure restored mtDNA damage to basal levels. (**A**) 24 h treatment with a LRRK2 kinase inhibitor (1 μM) is sufficient to reverse mtDNA damage in LRRK2 G2019S-patient derived lymphoblastoid cells (LCLs). (*$P < 0.05$, determined by one-way ANOVA with a Tukey's posthoc comparison). Of note, the controls showed a trend towards fewer mtDNA damage lesions after LRRK2 kinase inhibitor treatment than compared to vehicle. This may reflect an enhanced DNA repair response (22). (**B**) No difference in mtDNA copy was detected. The PCR based assay was performed in technical triplicate (twice) for each biological replicate. Control ($n = 3$) and G2019S patient derived LCLs ($n = 3$). Data are presented as mean ± SEM.

Table 2. Fibroblasts: genotypes, individual age at biopsy, gender, clinical status, mtDNA damage levels and mtDNA copy number

ID #	Age at biopsy	Genetic mutation	Clinical Status	Gender	mtDNA damage	mtDNA copy #
2070	35	None detected	Unaffected	male	0.0 lesions/10kb	1.0
1775	35	*LRRK2* G2019S heterozygous	Unaffected	male	0.01 lesions/10kb	0.99
1790	61	None detected	Unaffected	male	0.0 lesions/10kb	1.0
1859	68	*LRRK2* G2019S heterozygous	Affected	male	−0.02 lesions/10kb	0.97
1615	92	None detected	Unaffected	female	0.0 lesions/10kb	1.0
1824	90	*LRRK2* G2019S heterozygous	Unaffected	male	0.02 lesions/10kb	1.02

(cortical). Maintenance of the cultures took place at 37 °C with 5% CO_2/95% air. For the first 48 h, midbrain cultures were maintained in MEM (Life Technologies) containing 2% heat-inactivated fetal bovine serum (Cellgro), 2% heat-inactivated horse serum (Life Technologies), 1 g/L glucose (Sigma), 2 mM glutamax (Life Technologies), 1 mM sodium pyruvate (Cellgro), 100 μM non-essential amino acids (Cellgro), 50 U/ml penicillin and 50 μg/ml streptomycin (Corning). Of note, there are ∼ 5% tyrosine hydroxylase (TH) immunoreactive neurons in this culture system (56). The culture medium was then changed to 0.5 ml/well of fresh serum-free Neurobasal medium containing 2% B27 supplement (Life Technologies), 2 mM glutamax I (Life Technologies), 0.5 mg/ml albumax I (Life Technologies) and penicillin-streptomycin (Corning).

Primary midbrain or cortical neuron cultures on DIV 7 were transduced for 18 h or 24 h with Green Fluorescence Protein (GFP) or human LRRK2-GFP fusions of wild type, G2019S (increased kinase activity mutant) or D1994A (kinase dead) via BacMam technology (Life Technologies) which utilizes a modified insect cell baculovirus. Pilot studies determined optimal concentrations of each GFP or LRRK2 BacMam vector to be (1% v/v GFP, 10% v/v WT and G2019S, 5% v/v D1994A). LRRK2 lentiviral vector-mediated transduction with reagents available through the Leuven Viral Vector Core were not feasible due to transduction efficiencies < 1%.

Western blot analysis

Western blot analysis was performed on both primary midbrain neuronal cultures and lymphoblastoid cell lines (LCLs). Primary neuronal cultures were scraped using a Falcon cell scraper and collected in 1X sample buffer and protease inhibitor cocktail (Sigma-Aldrich), homogenized using a Misonix sonicator 3000 (intensity 2, three times), NuPAGE® Sample loading dye and

reducing agent was added to the sample and then heated at 100 °C for 5 min. LCLs were resuspended in a buffer reported previously (39). For our investigations, the following antibodies were used: anti-LRRK2 (Abcam c41-2, ab133474, 1: 2000), (N241A/34, NeuroMab, 75-253, 1: 2000), anti-tubulin β3 TUBB3 (BioLegend, 801201, 1: 1000), mouse anti-β-actin (Novus, 8H10D10, 1: 5, 000), rabbit anti-LRRK2 pS935 (abcam, 1: 1000), rabbit anti-β-actin (Abcam, ab8227, 1: 5000). The blots were then probed with fluorescently labeled secondary antibodies (Li-Cor antibodies). The fluorescent signal intensities were quantified using an Odyssey Imaging scanner (Li-Cor, Lincoln, Nebraska). The quantitative analysis was performed normalizing the fluorescent signal intensity of the protein of interest with the fluorescent intensity of either TUJ1 or β-actin. For primary midbrain or cortical neuron cultures all values are averaged from at least three independent biological replicates. For LCLs, all values are averaged from three experimental replicates within a cell line and at least three controls and three PD cell lines.

Cell viability

Primary midbrain or cortical neuron cultures were plated in 96-well culture plates at a density of 80, 000 cells/well pre-coated with PDL (0.1 mg/ml). The entire outer part of the plate (A and H plus 1 and 12) was not used to minimize edge effects. Cell viability was measured using the Live/Dead Viability Kit (Life Technologies). Fluorescence was measured at excitation of 485 nm and 530 nm emission using a SpectraMax Gemini (Molecular Devices). All values were averaged from at least 12 wells from three independent biological experiments.

Measurement of neurite outgrowth

Measurement of neurite outgrowth was performed using the Molecular Probes® Neurite Outgrowth Staining Kit following the live-cell straining protocol (ThermoFisher Scientific, A15001). Primary midbrain or cortical neuronal cultures were plated in 96-well culture plates at a density of 80, 000/well pre-coated with PDL (0.1 mg/ml). Fluorescence was measured at an excitation of 555 nm and 565 nm emission using a SpectraMax Gemini (Molecular Devices). All values were averaged from at least 12 wells from three independent biological experiments.

RNA isolation and quantitative real-time PCR

For primary neuron cultures, six 24-well coverslips were combined for each treatment analysis. Cells were trypsinized and centrifuged for three min at 1200 x g. Cells were then washed in cold 1X PBS, centrifuged for three min at 1200 x g. Cell pellets were stored at −80 °C. RNA was extracted using the RNeasy Mini Kit (QIAGEN). 2 μg of total RNA were used for cDNA synthesis using the SABiosciences RT^2 First Strand Kit (Qiagen). Quantitative Real-Time PCR (QRT-PCR) was performed using the SYBR Green Master Mix (Applied Biosystems) and validated primers for human *LRRK2*, human *GAPDH*, rat *LRRK2* and rat *RPL19* (QIAGEN catalogue numbers respectively, PPH13710A, PPH00150F, PPR53908A and PPR43077A). A two-step real-time PCR reaction was performed starting at 95 °C (10 min) for 1 cycle and followed by 95 °C (15 s) and 60 °C (1 min) for 40 cycles. Each sample was run in triplicate. Results were analyzed using the ΔΔCt method.

Seahorse cellular respiration

Cellular oxygen consumption rate (OCR) was measured using the Seahorse XF96 (Seahorse Bioscience™) extracellular flux analyzer as described (22) with minor modifications. Intact primary midbrain neuronal cultures were cultured on 96-well Seahorse XF96 plates seeded at 80, 000 cells/well for 1 week in growth medium and then transduced with BacMam virus for 24 h. Media containing final optimized concentrations of 10 μM oligomycin, 300 nM carbonyl cyanide 4-(trifluoromethoxy) phenylhydrazone (FCCP), 1 μM rotenone and 1 μM antimycin A were pre-loaded into the drug delivery system. Plates were then incubated in Calibrant medium (Seahorse Bioscience) for at least 30 min. Once the basal OCR was measured, the compounds were added sequentially and the effects on OCR measured every 8 min. All basal OCR measurements were within a range of 75-150 pmol O_2/min, which is in the linear range for assessment. At the end of the respiration measurements, plates were fixed in 4% paraformaldehyde for 10 min at RT and quantitative MAP2 in-cell Western blots were performed for normalization (58). Briefly, neuronal cells were probed with a rabbit anti-MAP2 (Millipore, 1: 1000). A Li-Cor IR-800 donkey anti-rabbit secondary was then applied at 1: 5000. The 96-well plate was scanned on a Li-Cor Odyssey imaging system (with care to avoid saturation) and infrared signal quantified using LiCor imaging software. The individual well respiration measurements were normalized by their respective MAP2 immunofluorescence intensity levels.

DNA isolation and quantification

DNA isolation and quantification was performed as previously described (20–22) using a high molecular weight genomic DNA purification kit according to the manufacturer's protocol (QIAGEN Genomic tip either 20/G or 100/G) and Quant-iT Picogreen dsDNA quantification. Following genomic DNA isolation, the purity and quality was assessed using a Nanodrop (ND-1000).

Quantifying mtDNA damage with a PCR-based assay

The PCR-based assay to calculate mitochondrial DNA lesion frequency was performed as previously described (20–22) with minor modifications. Reaction mixtures used KAPA Long Range HotStart DNA Polymerase (KAPABiosystems) in a 96-well platform. Primers used for human and rat short and long amplicons can be found in (59). Each biological DNA sample was performed in triplicate on two independent days (for a total of 6 PCR reactions).

Healthy subject and patient-derived cells: fibroblasts and lymphoblastoid cell lines

LRRK2 G2019S PD patient ($n = 6$) and healthy subject control ($n = 6$)-derived lymphoblastoid cell lines (LCL) were derived at the Parkinson's Institute or obtained from the NINDS Coriell biorepository (ID numbers are indicated in Table 1). There was not a statistical difference in the ages between the LRRK2 G2019S PD patient and healthy control subjects ($P = 0.5181$). LCLs were cultured in RPMI-1640 (Sigma-Aldrich), 15% FBS (ThermoFisher) and 0.5% Penicillin/Streptomycin (Corning). LRRK2 G2019S PD patient ($n = 3$) and healthy subject control ($n = 3$)-derived fibroblast cell lines were derived from skin biopsies obtained at the Parkinson's Institute (60) and are described in Table 2. Subjects gave informed consent to the study and the protocol was approved by local IRB and annually reviewed. Fibroblast cell lines were age and gender matched where possible. Using standard

culture techniques fibroblast lines were cultured in DMEM high glucose (Thermo Fisher Scientific, SH30081.02), 20% fetal bovine serum (Thermo Fisher Scientific, 10438026), 1x Glutamax (Thermo Fisher Scientific, 35050-061), 1x non-essential amino acids (Thermo Fisher Scientific, 11140-050), 1X Penicillin/Streptomycin (Thermo Fisher Scientific, 15140-122) and 1x sodium pyruvate (Thermo Fisher Scientific, 11360070). Cell passage number did not exceed 20.

Digital PCR method and primer-probe assays

A primer: probe ratio of 3: 1 was used for all assays, except for the primer-limited form (ND1pl), which were used at 1: 1 for mtDNA quantitation. All primers and probes were from IDT (Coralville, Iowa).

ND1 assay
Probe: 5'-HEX/CCATCACCC/ZEN/TCTACATCACCGCCC/3IABkFQ/-3'
Primer 1: 5'-GAGCGATGGTGAGAGCTAAGGT-3'
Primer 2: 5'-CCCTAAAACCCGCCACATCT-3'
ND4 assay
Probe: 5'-FAM/CCGACATCA/ZEN/TTACCGGGTTTTCCTCTTG/3IABkFQ/-3'
Primer 1: 5'-ACAATCTGATGTTTTGGTTAAACTATATTT-3'
Primer 2: 5'-CCATTCTCCTCCTATCCCTCAAC-3'

DNA from control and LRRK2 G2019S patient-derived LCLs were used as templates for digital PCR (dPCR) analysis using multiplex ND4 and ND1 primer probes on the QuantStudio 3D Digital PCR System and with supplied reagents (Applied Biosystems, Waltham, MA) according to previously published protocols (49).

Statistical analysis

The software GraphPad Prism was used for statistical computation. Data were analyzed by either Student two tailed, unpaired *t*-test or ANOVA with Tukey's post-hoc analysis and $P < 0.05$ was deemed significant. For all graphs, the bars represent mean ± standard error of the mean (SEM).

Supplementary Material

Supplementary Material is available at *HMG* online.

Acknowledgements

We would like to thanks members of the Sanders, Greenamyre, Schuele and Kaufman laboratories. We thank Connie Marras for contribution of blood samples for the generation of lymphoblastoid cell lines.

Conflict of Interest statement. None declared.

Funding

William N. & Bernice E. Bumpus Foundation [L.H.S.], Pittsburgh Claude D. Pepper OAIC [AG024827 to L.H.S., KL2 support], Michael J Fox Foundation [L.H.S., J.T.G, B.S.], and National Institutes of Health [R01GM110424 to B.A.K.].

References

1. Hernandez, D.G., Reed, X. and Singleton, A.B. (2016) Genetics in Parkinson disease: Mendelian versus non-Mendelian inheritance. *J. Neurochem.*, **139 Suppl 1**, 59–74.
2. Gilligan, P.J. (2015) Inhibitors of leucine-rich repeat kinase 2 (LRRK2): progress and promise for the treatment of Parkinson's disease. *Curr. Top. Med. Chem.*, **15**, 927–938.
3. Fraser, K.B., Rawlins, A.B., Clark, R.G., Alcalay, R.N., Standaert, D.G., Liu, N., Parkinson's Disease Biomarker Program, C. and West, A.B. (2016) Ser(P)-1292 LRRK2 in urinary exosomes is elevated in idiopathic Parkinson's disease. *Mov. Disord.*, **31**, 1543–1550.
4. Jaleel, M., Nichols, R.J., Deak, M., Campbell, D.G., Gillardon, F., Knebel, A. and Alessi, D.R. (2007) LRRK2 phosphorylates moesin at threonine-558: characterization of how Parkinson's disease mutants affect kinase activity. *Biochem. J.*, **405**, 307–317.
5. Greggio, E., Jain, S., Kingsbury, A., Bandopadhyay, R., Lewis, P., Kaganovich, A., van der Brug, M.P., Beilina, A., Blackinton, J., Thomas, K.J. *et al.* (2006) Kinase activity is required for the toxic effects of mutant LRRK2/dardarin. *Neurobiol. Dis.*, **23**, 329–341.
6. Smith, W.W., Pei, Z., Jiang, H., Dawson, V.L., Dawson, T.M. and Ross, C.A. (2006) Kinase activity of mutant LRRK2 mediates neuronal toxicity. *Nat. Neurosci.*, **9**, 1231–1233.
7. West, A.B. (2015) Ten years and counting: moving leucine-rich repeat kinase 2 inhibitors to the clinic. *Mov. Disord.*, **30**, 180–189.
8. Deng, X., Choi, H.G., Buhrlage, S.J. and Gray, N.S. (2012) Leucine-rich repeat kinase 2 inhibitors: a patent review (2006–2011). *Expert Opin. Ther. Pat.*, **22**, 1415–1426.
9. Kethiri, R.R. and Bakthavatchalam, R. (2014) Leucine-rich repeat kinase 2 inhibitors: a review of recent patents (2011–2013). *Expert Opin. Ther. Pat.*, **24**, 745–757.
10. Sheng, Z., Zhang, S., Bustos, D., Kleinheinz, T., Le Pichon, C.E., Dominguez, S.L., Solanoy, H.O., Drummond, J., Zhang, X., Ding, X. *et al.* (2012) Ser1292 autophosphorylation is an indicator of LRRK2 kinase activity and contributes to the cellular effects of PD mutations. *Sci. Transl. Med.*, **4**, 164ra161.
11. Yao, C., Johnson, W.M., Gao, Y., Wang, W., Zhang, J., Deak, M., Alessi, D.R., Zhu, X., Mieyal, J.J., Roder, H. *et al.* (2013) Kinase inhibitors arrest neurodegeneration in cell and *C. elegans* models of LRRK2 toxicity. *Hum. Mol. Genet.*, **22**, 328–344.
12. Reinhardt, P., Schmid, B., Burbulla, L.F., Schondorf, D.C., Wagner, L., Glatza, M., Hoing, S., Hargus, G., Heck, S.A., Dhingra, A. *et al.* (2013) Genetic correction of a LRRK2 mutation in human iPSCs links parkinsonian neurodegeneration to ERK-dependent changes in gene expression. *Cell Stem Cell*, **12**, 354–367.
13. Cooper, O., Seo, H., Andrabi, S., Guardia-Laguarta, C., Graziotto, J., Sundberg, M., McLean, J.R., Carrillo-Reid, L., Xie, Z., Osborn, T. *et al.* (2012) Pharmacological rescue of mitochondrial deficits in iPSC-derived neural cells from patients with familial Parkinson's disease. *Sci. Transl. Med.*, **4**, 141ra190.
14. Lee, B.D., Shin, J.H., VanKampen, J., Petrucelli, L., West, A.B., Ko, H.S., Lee, Y.I., Maguire-Zeiss, K.A., Bowers, W.J., Federoff, H.J. *et al.* (2010) Inhibitors of leucine-rich repeat kinase-2 protect against models of Parkinson's disease. *Nat. Med.*, **16**, 998–1000.
15. Fuji, R.N., Flagella, M., Baca, M., Baptista, M.A., Brodbeck, J., Chan, B.K., Fiske, B.K., Honigberg, L., Jubb, A.M., Katavolos, P. *et al.* (2015) Effect of selective LRRK2 kinase inhibition on nonhuman primate lung. *Sci. Transl. Med.*, **7**, 273ra215.
16. Lobbestael, E., Civiero, L., De Wit, T., Taymans, J.M., Greggio, E. and Baekelandt, V. (2016) Pharmacological LRRK2 kinase inhibition induces LRRK2 protein destabilization and proteasomal degradation. *Sci. Rep.*, **6**, 33897.

17. Jeppesen, D.K., Bohr, V.A. and Stevnsner, T. (2011) DNA repair deficiency in neurodegeneration. *Prog. Neurobiol.*, **94**, 166–200.
18. Hoch, N.C., Hanzlikova, H., Rulten, S.L., Tetreault, M., Komulainen, E., Ju, L., Hornyak, P., Zeng, Z., Gittens, W., Rey, S.A. *et al.* (2017) XRCC1 mutation is associated with PARP1 hyperactivation and cerebellar ataxia. *Nature*, **541**, 87–91.
19. Ross, C.A. and Truant, R. (2017) DNA repair: A unifying mechanism in neurodegeneration. *Nature*, **541**, 34–35.
20. Sanders, L.H., Howlett, E.H., McCoy, J. and Greenamyre, J.T. (2014) Mitochondrial DNA damage as a peripheral biomarker for mitochondrial toxin exposure in rats. *Toxicol. Sci.*, **142**, 395–402.
21. Sanders, L.H., Laganiere, J., Cooper, O., Mak, S.K., Vu, B.J., Huang, Y.A., Paschon, D.E., Vangipuram, M., Sundararajan, R., Urnov, F.D. *et al.* (2014) LRRK2 mutations cause mitochondrial DNA damage in iPSC-derived neural cells from Parkinson's disease patients: reversal by gene correction. *Neurobiol. Dis.*, **62**, 381–386.
22. Sanders, L.H., McCoy, J., Hu, X., Mastroberardino, P.G., Dickinson, B.C., Chang, C.J., Chu, C.T., Van Houten, B. and Greenamyre, J.T. (2014) Mitochondrial DNA damage: molecular marker of vulnerable nigral neurons in Parkinson's disease. *Neurobiol. Dis.*, **70**, 214–223.
23. Van Laar, V.S., Arnold, B., Cassady, S.J., Chu, C.T., Burton, E.A. and Berman, S.B. (2011) Bioenergetics of neurons inhibit the translocation response of Parkin following rapid mitochondrial depolarization. *Hum. Mol. Genet.*, **20**, 927–940.
24. Hermanson, S.B., Carlson, C.B., Riddle, S.M., Zhao, J., Vogel, K.W., Nichols, R.J., Bi, K. and Kahle, P.J. (2012) Screening for novel LRRK2 inhibitors using a high-throughput TR-FRET cellular assay for LRRK2 Ser935 phosphorylation. *PLoS One*, **7**, e43580.
25. Li, L.H., Qin, H.Z., Wang, J.L., Wang, J., Wang, X.L. and Gao, G.D. (2009) Axonal degeneration of nigra-striatum dopaminergic neurons induced by 1-methyl-4-phenyl-1, 2, 3, 6-tetrahydropyridine in mice. *J. Int. Med. Res.*, **37**, 455–463.
26. Herkenham, M., Little, M.D., Bankiewicz, K., Yang, S.C., Markey, S.P. and Johannessen, J.N. (1991) Selective retention of MPP+ within the monoaminergic systems of the primate brain following MPTP administration: an in vivo autoradiographic study. *Neuroscience*, **40**, 133–158.
27. Skibinski, G., Nakamura, K., Cookson, M.R. and Finkbeiner, S. (2014) Mutant LRRK2 toxicity in neurons depends on LRRK2 levels and synuclein but not kinase activity or inclusion bodies. *J. Neurosci.*, **34**, 418–433.
28. MacLeod, D., Dowman, J., Hammond, R., Leete, T., Inoue, K. and Abeliovich, A. (2006) The familial Parkinsonism gene LRRK2 regulates neurite process morphology. *Neuron*, **52**, 587–593.
29. Rudenko, I.N., Kaganovich, A., Hauser, D.N., Beylina, A., Chia, R., Ding, J., Maric, D., Jaffe, H. and Cookson, M.R. (2012) The G2385R variant of leucine-rich repeat kinase 2 associated with Parkinson's disease is a partial loss-of-function mutation. *Biochem. J.*, **446**, 99–111.
30. Sanders, L.H. and Greenamyre, J.T. (2013) Oxidative damage to macromolecules in human Parkinson disease and the rotenone model. *Free Radic. Biol. Med.*, **62**, 111–120.
31. De Miranda, B.R., Van Houten, B. and Sanders, L.H. (2016) *Mitochondrial Mechanisms of Degeneration and Repair in Parkinson's Disease*. Buhlman, Lori M. (Ed.), Springer International Publishing, Switzerland.
32. Rudenko, I.N., Kaganovich, A., Langston, R.G., Beilina, A., Ndukwe, K., Kumaran, R., Dillman, A.A., Chia, R. and Cookson, M.R. (2017) The G2385R risk factor for Parkinson's disease enhances CHIP-dependent intracellular degradation of LRRK2. *Biochem. J.*, **474**, 1547–1558.
33. Martin, I., Kim, J.W., Dawson, V.L. and Dawson, T.M. (2014) LRRK2 pathobiology in Parkinson's disease. *J. Neurochem.*, **131**, 554–565.
34. Chan, B.K., Estrada, A.A., Chen, H., Atherall, J., Baker-Glenn, C., Beresford, A., Burdick, D.J., Chambers, M., Dominguez, S.L., Drummond, J. *et al.* (2013) Discovery of a highly selective, brain-penetrant aminopyrazole LRRK2 inhibitor. *ACS Med. Chem. Lett.*, **4**, 85–90.
35. Choi, H.G., Zhang, J., Deng, X., Hatcher, J.M., Patricelli, M.P., Zhao, Z., Alessi, D.R. and Gray, N.S. (2012) Brain penetrant LRRK2 inhibitor. *ACS Med. Chem. Lett.*, **3**, 658–662.
36. Kavanagh, M.E., Doddareddy, M.R. and Kassiou, M. (2013) The development of CNS-active LRRK2 inhibitors using property-directed optimisation. *Bioorg. Med. Chem. Lett.*, **23**, 3690–3696.
37. Doggett, E.A., Zhao, J., Mork, C.N., Hu, D. and Nichols, R.J. (2012) Phosphorylation of LRRK2 serines 955 and 973 is disrupted by Parkinson's disease mutations and LRRK2 pharmacological inhibition. *J. Neurochem.*, **120**, 37–45.
38. Dzamko, N., Deak, M., Hentati, F., Reith, A.D., Prescott, A.R., Alessi, D.R. and Nichols, R.J. (2010) Inhibition of LRRK2 kinase activity leads to dephosphorylation of Ser(910)/Ser(935), disruption of 14-3-3 binding and altered cytoplasmic localization. *Biochem. J.*, **430**, 405–413.
39. Reynolds, A., Doggett, E.A., Riddle, S.M., Lebakken, C.S. and Nichols, R.J. (2014) LRRK2 kinase activity and biology are not uniformly predicted by its autophosphorylation and cellular phosphorylation site status. *Front. Mol. Neurosci.*, **7**, 54.
40. Chia, R., Haddock, S., Beilina, A., Rudenko, I.N., Mamais, A., Kaganovich, A., Li, Y., Kumaran, R., Nalls, M.A. and Cookson, M.R. (2014) Phosphorylation of LRRK2 by casein kinase 1alpha regulates trans-Golgi clustering via differential interaction with ARHGEF7. *Nat. Commun.*, **5**, 5827.
41. Smith, G.A., Jansson, J., Rocha, E.M., Osborn, T., Hallett, P.J. and Isacson, O. (2016) Fibroblast biomarkers of sporadic Parkinson's disease and LRRK2 kinase inhibition. *Mol. Neurobiol.*, **53**, 5161–5177.
42. Kuss, M., Adamopoulou, E. and Kahle, P.J. (2014) Interferon-gamma induces leucine-rich repeat kinase LRRK2 via extracellular signal-regulated kinase ERK5 in macrophages. *J. Neurochem.*, **129**, 980–987.
43. Rosenbusch, K.E. and Kortholt, A. (2016) Activation mechanism of LRRK2 and its cellular functions in Parkinson's disease. *Parkinsons Dis.*, **2016**, 7351985.
44. Steger, M., Tonelli, F., Ito, G., Davies, P., Trost, M., Vetter, M., Wachter, S., Lorentzen, E., Duddy, G., Wilson, S. *et al.* (2016) Phosphoproteomics reveals that Parkinson's disease kinase LRRK2 regulates a subset of Rab GTPases. *Elife*, **5**.
45. Tang, F.L., Liu, W., Hu, J.X., Erion, J.R., Ye, J., Mei, L. and Xiong, W.C. (2015) VPS35 Deficiency or mutation causes dopaminergic neuronal loss by impairing mitochondrial fusion and function. *Cell Rep.*, **12**, 1631–1643.
46. Atashrazm, F. and Dzamko, N. (2016) LRRK2 inhibitors and their potential in the treatment of Parkinson's disease: current perspectives. *Clin. Pharmacol.*, **8**, 177–189.
47. Yakes, F.M. and Van Houten, B. (1997) Mitochondrial DNA damage is more extensive and persists longer than nuclear DNA damage in human cells following oxidative stress. *Proc. Natl. Acad. Sci. U S A*, **94**, 514–519.
48. Vermulst, M., Wanagat, J. and Loeb, L.A. (2009) On mitochondria, mutations, and methodology. *Cell Metabol.*, **10**, 437.

49. Belmonte, F.R., Martin, J.L., Frescura, K., Damas, J., Pereira, F., Tarnopolsky, M.A. and Kaufman, B.A. (2016) Digital PCR methods improve detection sensitivity and measurement precision of low abundance mtDNA deletions. *Sci. Rep.*, **6**, 25186.
50. Valente, W.J., Ericson, N.G., Long, A.S., White, P.A., Marchetti, F. and Bielas, J.H. (2016) Mitochondrial DNA exhibits resistance to induced point and deletion mutations. *Nucleic Acids Res.*, **44**, 8513–8524.
51. Kalia, L.V., Lang, A.E., Hazrati, L.N., Fujioka, S., Wszolek, Z.K., Dickson, D.W., Ross, O.A., Van Deerlin, V.M., Trojanowski, J.Q., Hurtig, H.I. *et al.* (2015) Clinical correlations with Lewy body pathology in LRRK2-related Parkinson disease. *JAMA Neurol.*, **72**, 100–105.
52. Surmeier, D.J., Obeso, J.A. and Halliday, G.M. (2017) Selective neuronal vulnerability in Parkinson disease. *Nat. Rev. Neurosci.*, **18**, 101–113.
53. Horowitz, M.P., Milanese, C., Di Maio, R., Hu, X., Montero, L.M., Sanders, L.H., Tapias, V., Sepe, S., van Cappellen, W.A., Burton, E.A. *et al.* (2011) Single-cell redox imaging demonstrates a distinctive response of dopaminergic neurons to oxidative insults. *Antioxid. Redox. Signal.*, **15**, 855–871.
54. Hastings, T.G. (2009) The role of dopamine oxidation in mitochondrial dysfunction: implications for Parkinson's disease. *J. Bioenerg. Biomembr.*, **41**, 469–472.
55. Perera, G., Ranola, M., Rowe, D.B., Halliday, G.M. and Dzamko, N. (2016) Inhibitor treatment of peripheral mononuclear cells from Parkinson's disease patients further validates LRRK2 dephosphorylation as a pharmacodynamic biomarker. *Sci. Rep.*, **6**, 31391.
56. Tapias, V., Greenamyre, J.T. and Watkins, S.C. (2013) Automated imaging system for fast quantitation of neurons, cell morphology and neurite morphometry in vivo and in vitro. *Neurobiol. Dis.*, **54**, 158–168.
57. Tapias, V., Hu, X., Luk, K.C., Sanders, L.H., Lee, V.M. and Greenamyre, J.T. (2017) Synthetic alpha-synuclein fibrils cause mitochondrial impairment and selective dopamine neurodegeneration in part via iNOS-mediated nitric oxide production. *Cell. Mol. Life Sci.*, **74**, 2851–2874.
58. Larsen, N.J., Ambrosi, G., Mullett, S.J., Berman, S.B. and Hinkle, D.A. (2011) DJ-1 knock-down impairs astrocyte mitochondrial function. *Neuroscience*, **196**, 251–264.
59. Ayala-Torres, S., Chen, Y., Svoboda, T., Rosenblatt, J. and Van Houten, B. (2000) Analysis of gene-specific DNA damage and repair using quantitative polymerase chain reaction. *Methods*, **22**, 135–147.
60. Vangipuram, M., Ting, D., Kim, S., Diaz, R. and Schüle, B. (2013) Skin punch biopsy explant culture for derivation of primary human fibroblasts. *J. Vis. Exp.*, **77**, e3779.